HHS Public Access

Author manuscript

AAPS J. Author manuscript; available in PMC 2022 June 24.

Published in final edited form as:

AAPS J. ; 23(4): 88. doi:10.1208/s12248-021-00619-4.

Formoterol PLGA-PEG Nanoparticles Induce Mitochondrial Biogenesis in Renal Proximal Tubules

Ernest L. Vallorz[1], **Karen Blohm-Mangone**[1], **Rick G. Schnellmann**[1,2,3,4], **Heidi M. Mansour**[1,2,3,5,6]

[1]Department of Pharmacology and Toxicology, The University of, Arizona College of Pharmacy, Tucson, Arizona 85721, USA.

[2]Department of Medicine, The University of Arizona College of, Medicine, Tucson, Arizona 85724, USA.

[3]BIO5 Institute, The University of Arizona, Tucson, Arizona 85719, USA.

[4]Southern Arizona VA Health Care System, Tucson, Arizona 85723, USA.

[5]Colleges of Pharmacy & Medicine, The University of Arizona, 1703, E. Mabel St, Tucson, Arizona 85721-0207, USA.

Abstract

Formoterol is a long-acting β_2 agonist (LABA). Agonism of the β_2-adrenergic receptor by formoterol is known to stimulate mitochondrial biogenesis (MB) in renal proximal tubules and recover kidney function. However, formoterol has a number of cardiovascular side effects that limits its usage. The goal of this study was to design and develop an intravenous biodegradable and biocompatible polymeric nanoparticle delivery system that targets formoterol to the kidney. Poly(ethylene glycol) methyl ether-blockpoly(lactide-co-glycolide) nanoparticles containing encapsulated formoterol were synthesized by a modified single-emulsion solvent evaporation technique resulting in nanoparticles with a median hydrodynamic diameter of 442 ± 17 nm. Using primary cell cultures of rabbit renal proximal tubular cells (RPTCs), free formoterol, encapsulated formoterol polymeric nanoparticles, and drug-free polymeric nanoparticles were biocompatible and not cytotoxic over a wide concentration range. In healthy male mice, polymeric nanoparticles were shown to localize in tubules of the renal cortex and improved the renal localization of encapsulated formoterol compared to the free formoterol. At a lower total formoterol dose, the nanoparticle localization resulted in increased expression of peroxisome proliferator-activated receptor-γ coactivator-1α (PGC-1α), the master regulator of MB, and increased electron transport chain proteins, markers of MB. This was confirmed by direct visual quantification of mitochondria and occurred with both free formoterol and the encapsulated

[6]To whom correspondence should be addressed. (mansour@pharmacy.arizona.edu).

AUTHOR CONTRIBUTIONS

Ernest L. Vallorz: Conceptualization, methodology, data acquisition, interpretation, analysis, writing — original draft. Karen Blohm-Mangone: methodology, data acquisition. Rick G. Schnellmann: conceptualization; methodology; interpretation; analysis; writing — review and editing; resources; funding acquisition; resources; supervision; project administration. Heidi M. Mansour: conceptualization; methodology; interpretation; analysis; writing — review and editing; resources; supervision; project administration

DECLARATIONS

Conflict of interest The authors declare no competing interests.

formoterol polymeric nanoparticles. At the same time, localization of nanoparticles to the kidneys resulted in reduced induction of MB markers in the heart. These new nanoparticles effectively target formoterol to the kidney and successfully produce MB in the kidney.

Keywords

controlled drug release; formoterol; mitochondrial biogenesis; nanoparticles kidney; primary cell culture

INTRODUCTION

Mitochondrial dysfunction is a mediator of both acute and chronic renal injury, including drug- and toxicant-induced renal injury, ischemia-reperfusion injury, and diabetic kidney disease (1–5). Mitochondrial dysfunction as a result of oxidant injury results in a decrease in the number and functionality of renal proximal tubule cell (RPTC) mitochondria as well as inhibition of ATP-dependent cellular repair processes (6). This continual energy depletion and disruption of mitochondrial homeostasis hinders recovery and can lead to irreversible tissue and organ injury (1, 7–9). As such, the development of therapies that can promote mitochondrial function and repair is a critical area of research.

Mitochondrial biogenesis (MB) has been shown to promote recovery of mitochondrial and cellular function (6, 10–12) via induction of the peroxisome proliferator-activated receptor-γ coactivator-1α (PGC-1α), which is expressed in highly metabolic tissues such as the heart, skeletal muscle, and kidneys (13). Increased expression of PGC-1α following formoterol treatment of RPTC showed increased mitochondrial DNA copy number as well as increased expression of electron transport chain (ETC) proteins and elevated mitochondrial respiration rate (14). Formoterol fumarate dihydrate is a US Food and Drug Administration (FDA)-approved β_2-adrenergic receptor agonist for the treatment of asthma and obstructive pulmonary disease via inhalation. Our lab has shown formoterol to be a potent inducer of PGC-1α and MB in RPTC (15, 16). Additionally, formoterol treatment has been shown to improve renal function via MB in mouse models of acute kidney injury (15, 17, 18), glomerular disease (19), and maintaining mitochondrial dynamics in an early model of diabetic kidney disease (3).

The β_2-adrenergic receptor is ubiquitously expressed. In the kidney, the β_2-adrenergic receptor is increased in renal proximal tubules compared to other renal structures, making the tubules a primary target for a therapeutic effect (18, 20, 21). The prevalence of β_2-adrenergic receptors in other organs suggests that systemic formoterol exposure could have side effects and toxicity; for example, chronotropic and ionotropic effects of intravenous administration of formoterol (22–26). Systemic formoterol administration (≥0.003 mg/kg, s.c.) in Wistar rats showed an increase in heart rate of 100–150 bpm from baseline immediately following dosing, which persisted for up to 4 h. Additionally, the same study found formoterol resulted in a decrease in mean arterial pressure (MAP) at similar doses (27). As a result, translation of formoterol to the clinic is limited by its cardiovascular effects.

One potential means of addressing these side effects is the encapsulation of formoterol within a polymeric nanoparticle carrier using FDA-approved polymers that are biocompatible and biodegradable(28).These polymeric carriers offer the ability to encapsulate a wide variety of molecules including nucleic acids, proteins and peptides as well as small molecules and water-insoluble drugs(29). Furthermore, sustained drug release over prolonged period of time can be achieved using biocompatible and biodegradable polymers for injectable drug delivery systems(30, 31). PLGA is diblock copolymer(28) that is FDA-approved and has a long history of use in successfully marketed pharmaceutical products. Sustained drug release is achieved as drug molecules are released as the PLGA polymeric matrix slowly erodes by hydrolysis to lactic acid and glycolic acid monomers which are then renally excreted. PEGylation of the surface of a nanoparticle imparts several unique properties including prolonged circulation time as a result of evading phagocytosis and reducing uptake by the reticuloendothelial system (RES) (31, 32). Additionally, nanoparticles are able to modify the pharmacokinetics of entrapped drugs including enhanced membrane permeation, increased intracellular uptake, and prolonged circulation time and tissue retention (33–37).

Targeting of nanoparticles to the kidneys would allow for effective and efficient localization at the target site, as well as a reduction in the overall administered dose which is characteristic of nanoparticles and sustained release drug delivery systems (31, 37–42). Currently, there are no commercially available nano-pharmaceutical FDA-approved products that are indicated in the treatment of renal diseases (43), and few research studies have specifically targeted the renal tubules (42, 44–48). The purpose of this study was to design, develop, and characterize the physicochemical and sustained drug release properties of nanoparticles containing formoterol encapsulated in a polymeric matrix comprised of PLGA-PEG, which is FDA-approved, biocompatible, and biodegradable. Furthermore, effective renal localization and MB were successfully demonstrated *in vivo*. To the authors' knowledge, this is first to report on the generation of formoterol polymeric nanoparticles that demonstrate sustained drug release, renal localization, and MB *in vivo*.

EXPERIMENTAL: MATERIALS AND METHODS

Materials

Poly(ethylene glycol) methyl ether-block-poly(lactide-co-glycolide) (PLGA-PEG), lactide:glycolide ratio 50:50, PLGA average M_n 55,000, PEG average M_n 5,000, research grade was purchased from Sigma-Aldrich (St. Louis, MO). Formoterol fumarate dihydrate, 420.46 MW, > 98% pure was purchased from Sigma-Aldrich (St. Louis, MO). DMEM:F12, HEPES (Biochemistry grade), L-ascorbic acid-2-phosphate (Biochemistry grade), acetic acid (HPLC grade), CitriSolv™ (reagent grade), Alexa Fluor™ 594 secondary antibody, lectin phytohemagglutin-L conjugated to Alexa Fluor™ 488, and 4',6-diamidino-2-phenylindole dihydrochloride (DAPI) were purchased from Thermo Fisher (Waltham, MA). Poly(vinyl alcohol) (PVA) (89,000–98,000 MW, > 99% hydrolyzed, reagent grade), poloxamer 407 (~ 12,600 MW, reagent grade), potassium phosphate monobasic (> 99% purity), potassium phosphate dibasic (> 98% purity), formic acid (97.5–98.5% purity), hydrocortisone (molecular biology grade), selenium (99.99% pure),

human transferrin (molecular biology grade), bovine insulin (molecular biology grade), resazurin sodium salt (~ 80% dye content, molecular biology grade), neutral buffered formalin solution (10%, histology grade), Triton™ X-100 (molecular biology grade), sodium fluoride (≥ 99% purity), sodium orthovanadate (> 90% purity), protease inhibitor cocktail (molecular biology grade), hydrogen peroxide (3%, molecular biology grade), and Tween® 20 (molecular biology grade) were purchased from Sigma-Aldrich (St. Louis, MO). Chloroform (ACS grade), acetonitrile (ACS grade), and methanol (LCMS grade) were purchased from Spectrum Chemical Mfg. Corp. (Gardena, CA). Anti-polyethylene glycol (PEG), anti-mtND1, anti-NDUFS1, and anti-GAPDH primary antibodies were purchased from Abcam (Cambridge, MA). Anti-PGC-1α primary antibody was purchased from EMD Millipore (Billerica, MA). Anti-mouse and anti-rabbit secondary antibodies were purchased from Santa Cruz Biotechnology (Dallas, TX).

Methods

Synthesis and Physicochemical Characterization of Nanoparticles—Formoterol containing poly(ethylene glycol) methyl ether-block-poly(lactide-co-glycolide) (PLGA-PEG) (PLGA average M_n 55,000, PEG average M_n 5,000, Sigma-Aldrich, Saint Louis, MO) nanoparticles were synthesized using the oil-in-water single-emulsion solvent evaporation method (39). Briefly, 50 mg of PLGA-PEG was dissolved in a chloroform-acetonitrile 80:20 cosolvent. Formoterol fumarate dihydrate (Sigma-Aldrich, St. Louis, MO) was dissolved in glacial acetic acid (Thermo Fisher, Waltham, MA) (vendor, location), and then 10 μL of formoterol solution was added to form the organic phase. The resulting organic phase was then emulsified in an aqueous solution containing 3% PVA (Sigma-Aldrich, St. Louis, MO) using a microtip probe sonicator (Qsonica, Newtown, CT) at 60 W of energy output for 3 min over an ice bath. The single-emulsion was then diluted with 1% poloxamer 407 (Sigma-Aldrich, St. Louis, MO), and the organic cosolvent was removed using a rotary evaporator (RV10, IKA Works, Inc., Wilmington, NC) at 40°C for 40 min. The nanoparticle suspension was centrifuged at 15,000 relative centrifugal force (rcf) and washed thrice with distilled ultrapure water (18.2 MΩ.cm) (Milli-Q Plus, Millipore Sigma, Burlington, MA). Samples were lyophilized at −80°C under a vacuum < 0.133 mmHg (FreeZone 4.5 L, Labconco, Kansas City, MO) in 5% α-Trehalose (Acros Organics, Fair Lawn, NJ) and stored at −20°C until used in the physical characterization and *in vivo* animal studies.

An HPLC system (Alliance 2965, Waters, Milford, MA) with a UV dual-wavelength detector (Alliance 2487 Dual Wavelength Absorbance Detector, Waters, Milford, MA) with a C18-column (4.6 mm × 250 mm length, 5 μm pore size) (Phenomenex Torrance, CA) was used to quantify the amount of formoterol drug encapsulated within the polymeric nanoparticles. The mobile phase consisted of methanol (Spectrum Chemical MFG Corp., Gardena, CA) and 50 mM phosphoric acid (Sigma-Aldrich, St. Louis, MO) buffer with 1% acetic acid (Thermo Fisher, Waltham, MA) at a ratio of 65:35, 1.0 mL/min flow rate, and a column temperature of 40°C. The detection wavelength was 242 nm, and the injection volume was 10 μL. The % drug loading (DL) was calculated, as previously reported (49), using Eq. 1:

$$\mathrm{DL}(\%) = \frac{\text{the amount of formoterol assayed}}{\text{the total amount of nanoparticles in the preparation}} \times 100 \quad (1)$$

The % encapsulation (entrapment) efficiency (EE) was calculated, as previously reported (50) using Eq. 2:

$$\mathrm{EE}(\%) = \frac{\text{the amount of formoterol assayed}}{\text{the total amount of formoterol used in the preparation}} \times 100 \quad (2)$$

Analysis of the formoterol content in the renal cortex was carried out using d-6 formoterol (Clearsynth, Mumbai, India) as an internal standard. Homogenization and extraction of formoterol from the renal cortex in methanol followed by centrifugation and UPLC separation were carried out as previously described (51). Quantification of formoterol was measured using an Orbitrap Exploris 480 mass spectrometer (Thermo Finnigan, San Jose, CA) equipped with an electrospray ionization source, operated in positive ionization mode. The electrospray source was coupled online with Vanquish Duo an ultra-fast liquid chromatography system. The spray voltage was set to 3500 V, ion transfer tube temperature at 300°C, sheath gas pressure to 35 (Arb), ion sweep gas pressure to 0 (Arb), and aux gas pressure to 7 (Arb). Mass spectrometer was operated with tMS2 method, and detection was employed using nitrogen as the collision gas. Chromatographic separation was carried out onto C18 column (100 mm × 2.1 mm length, 1.7 μm pore size) (Phenomenex Torrance, CA). The UPLC mobile phases consisted of (A) 0.1% formic acid (Sigma-Aldrich, St. Louis, MO) in distilled water and (B) 0.1% formic acid (Sigma-Aldrich, St. Louis, MO) in acetonitrile (Spectrum Chemical MFG Corp., Gardena, CA). A gradient method of 10–98%B was run at a flow rate of 0.2 mL/min for 20 min. The injection volume was 2 μL. The raw data was processed by using TraceFinder 5.0 (Thermo Fisher, Waltham, MA).

Encapsulated formoterol in PLGA-PEG nanoparticles were suspended and diluted to a final concentration of 1 mg/mL with ultrapure water (18.2 MΩ.cm) (Milli-Q Plus, Millipore Sigma, Burlington, MA). Hydrodynamic particle size was determined by photon correlation spectroscopy using the Zetasizer Nano ZS (Malvern Instruments Ltd., Malvern, UK), using similar conditions and procedures published earlier (50). The nanoparticle suspension was evaluated using a scattering angle of 173° at a temperature of 25°C. A minimum of 10 measurements were taken per replicate, and samples were evaluated a minimum of 3 replicates ($n \geq 3$).

Zeta potential (ζ) measurements were carried out in 0.1× normal saline solution at 25°C and pH 7.2. The mean ζ was determined using the Zetasizer Nano ZS (Malvern Instruments Ltd., Malvern, UK) phase analysis light scattering technique.

The size and surface morphology of formoterol containing PLGA-PEG nanoparticles in the solid-state was visualized using SEM (FEI Inspect S SEM, FEI Company, Hillsboro, OR) at an accelerating voltage of 30 kV. Powders were deposited on double-sided carbon conductive adhesive tabs (Ted-Pella, Inc., Redding, CA, USA) attached to aluminum SEM stubs (Ted-Pella, Inc., Redding, CA, USA) and then sputter-coated (Anatech Hummer 6.2,

Union City, CA, USA) with gold for 90 s under Argon plasma to form a gold nanofilm before being loaded into the microscope, using conditions similar to previously reported (52).

In Vitro Drug Release—Using similar conditions as previously reported (53), formoterol-loaded polymeric nanoparticles were dispersed in 10 mL of phosphate-buffered saline (PBS) producing a final pH7.4 and incubated at 37°C under magnetic stirring. At determined time intervals up to 96 hours, aliquots were centrifuged at 10,000 rcf for 10 min. Supernatant was extracted and replaced with equal volume fresh PBS in order to maintain sink conditions. Samples were analyzed by HPLC, as described above. Nanoparticle release was determined in triplicate (n = 3). Data were plotted using Prism 9.0 (GraphPad Software, San Diego, CA, USA).

RPTC Viability—Female New Zealand white rabbits were purchased from Charles River (Oakwood, MI). RPTC were isolated, as previously described using the iron oxide perfusion method (54). The RPTCs were cultured on 35-mm tissue culture dishes with 1:1 DMEM:F-12 (without glucose, phenol red, or sodium pyruvate) as media supplemented with 15 mM HEPES buffer, 2.5 mM L-glutamine, 1 μM pyridoxine HCL, 15 mM sodium bicarbonate, and 6 mM lactate (Thermo Fisher, Waltham, MA). Hydrocortisone (50 nM, Sigma-Aldrich, St. Louis, MO), selenium (5 ng/mL, Sigma-Aldrich, St. Louis, MO), human transferrin (5 μg/mL, Sigma-Aldrich, St. Louis, MO), bovine insulin (10 nM, Sigma-Aldrich, St. Louis, MO), and L-ascorbic acid-2-phosphate (50 μM, Thermo Fisher, Waltham, MA) were added daily to fresh culture medium. Confluent cell monolayers were used for all experiments.

Cultured RPTCs were grown on 96-well plates at a cell density of 5×10^4 cells/cm^2 for 96 h. Cells were exposed to varying concentrations of free formoterol and formoterol-free polymeric nanoparticles. The treatments were each prepared by either dissolving free formoterol or suspending nanoparticles in culture media. Following 24 h of incubation at 37°C and 5% CO_2 with gentle shaking, the treatment was removed, and cells were rinsed and replenished with fresh media. Viability was determined by resazurin reduction assay, as described previously (52, 55). Detection was measured using Synergy H1 Multi-Mode Reader (BioTek Instruments, Inc., Winooski, VT) with 544 nm excitation and 590 nm emission wavelengths. Six replicates were used per rabbit and viability of the cells was calculated as follows:

$$\text{Relative viability } (\%) = \frac{\text{Sample fluorescence intensity}}{\text{Control fluorescence intensity}} \times 100\% \quad (3)$$

Renal Tubule Nanoparticle Uptake and (MB) in Mice—Male C57BL/6 mice (8–9 weeks of age) were obtained from Charles River (Oakwood, MI), housed in the University of Arizona Animal Care (UAC) Facility mouse room at a constant temperature of 22 ± 2°C with 12:12 h light-dark cycles, and received standard rodent food and water ad libitum. An acclimation period of least 1 week was completed before the mice were used in the experiments. A preliminary dose setting study was performed on a total of 3 (n =

3) different formoterol containing nanoparticle groups (0.3 mg/kg, 0.03 mg/kg, and 0.003 mg/kg formoterol) and one formoterol free drug group (0.3 mg/kg formoterol) with 5 mice per group (n = 5) and kidney tissue collected 1 h following administration. Nanoparticles were suspended in normal saline, and formoterol was prepared by dissolving formoterol fumarate dihydrate in normal saline at 0.03 mg/mL. Renal cortex was isolated and weighted. Formoterol content was determined per mg of cortical tissue by mass spectroscopy as described above. Following selection of the nanoparticle dose, a total of 3 groups (n = 3) were evaluated with 10 mice per group (n = 10). Mice were treated with normal saline drug-free vehicle, unencapsulated free formoterol (0.3 mg/kg/day) drug saline solution, or encapsulated formoterol polymeric nanoparticles (0.04 mg/kg/day) suspended in normal saline dosed via lateral tail vein injection. At 24 h post exposure, mice were euthanized, and the kidneys and heart were harvested. All experimental procedures were approved by the Institutional Animal Care and Use Committee (IACUC) at The University of Arizona in accordance with the guidelines set forth by the National Institutes of Health (NIH) *Guide for the Care and Use of Laboratory Animals*.

Kidney sections were harvested and fixed in 10% neutral buffered formalin solution (Sigma-Aldrich, St. Louis, MO) and embedded in paraffin. Embedded sections (5 μm thick) were deparaffinized using CitriSolv (Thermo Fisher, Waltham, MA) followed by rehydration in an ethanol gradient. Upon hydration, sections were permeabilized in 0.1% Trition X-100 (Sigma Aldrich, St. Louis, MO) for 10 min. Endogenous peroxidases were neutralized with 3% hydrogen peroxide (Sigma-Aldrich, St. Louis, MO). Slides were then blocked with normal horse serum in PBS for 1 h at room temperature. Polyethylene glycol (PEG) primary rat antibody (Abcam, Cambridge, MA) was added to slides at a 1:200 dilution and allowed to incubate overnight at 4°C in a humidified environment. Slides were washed with PBS and incubated for 1 h with Alexa Fluor 594 secondary antibody (Thermo Fisher, Waltham, MA) followed by lectin phytohemagglutin-L conjugated to Alexa Fluor 488 (Thermo Fisher, Waltham, MA) and DAPI nuclear dye (Thermo Fisher, Waltham, MA). VECTASHIELD Antifade Mounting Medium (Vector Laboratories, Burlington, CA) was applied to each section along with a glass coverslip. All images were acquired using the EVOS M5000 Imaging System (Thermo Fisher, Waltham, MA).

Protein was extracted from renal cortical tissue sections using radioimmunoprecipitation assay (RIPA) buffer (50 mM Tris-HCl, 150 mM NaCl, 0.1% SDS, 0.5% sodium deoxycholate and 1% Triton X-100, pH 7.4) with protease inhibitor cocktail (1:100), 1 mM sodium fluoride, and 1 mM sodium orthovanadate (Sigma Aldrich, St. Louis, MO) added prior to extraction. Equal protein quantities (10 μg) were loaded onto 4–15% SDS-PAGE gels, resolved by gel electrophoresis, and then transferred onto nitrocellulose membranes (0.45 μm pore size, Bio-Rad Laboratories, Inc, Hercules, CA). Membranes were blocked with 5% nonfat milk (Bio-Rad Laboratories, Inc, Hercules, CA) in Tris-buffered saline with Tween 20 (Sigma-Aldrich, St. Louis, MO) to prevent nonspecific binding and incubated at a temperature of 4°C for 18–24 h with primary antibody. Primary antibodies include PGC-1α (EMD Millipore, Billerica, MA), mt-ND1, NDUFS1, and GAPDH (Abcam, Cambridge, MA). Membranes were washed and incubated with the appropriate horseradish peroxidase-conjugated secondary antibody (Santa Cruz Biotechnology, Dallas, TX) for 1 h. Bound antibodies were visualized using enhanced chemiluminescence (Thermo Scientific,

Waltham, MA) and the GE ImageQuant LAS400 Biomolecular Imaging System (GE Healthcare, Marlborough, MA).

Renal cortical tissue sections were fixed in glutaraldehyde, stained, and sectioned for transmission electron microscopy as previously described (56). TEM was conducted using the FEI Tecnai Spirit microscope (FEI, Hillsboro, OR) operated at an accelerating voltage of 100 kV. Acquisition of images and counting of mitochondrial number and size was carried out by a researcher blinded to sample treatment group. A minimum of 250 mitochondria were counted per animal. Mitochondrial count and size were analyzed using MATLAB 9.9 (R2020b) (Mathworks, Natick, MA.).

Statistical Analysis—Comparison of the difference of between two groups was analyzed using two-tailed Student's t-test, while differences between three groups were performed by one-way analysis of variance (ANOVA) with Dunnett's post hoc test for comparisons (Prism 9.0, GraphPad Software, San Diego, CA, USA). In all cases p values of 0.05 or less were considered significant.

RESULTS

Synthesis and Physicochemical Characterization of Nanoparticles

Nanoparticles were synthesized by single-emulsion solvent evaporation. As shown in Fig. 1a, the median hydrodynamic particle size was 442 ± 17 nm (n = 3) with a polydispersity index of 0.1. The mean ζ-potential of the nanoparticles was 0.16 ± 0.04 mV (Fig.1c). The surface morphology of the nanoparticles was smooth, and particle shape was spherical, as seen in the SEM micrographs (Fig. 1b). These particles contained 1.6 μg formoterol per mg of nanoparticles with DL of 0.2 ± 0.04% drug loading and EE of 24 ± 5%.

In Vitro Drug Release

The *in vitro* drug release profile of formoterol containing nanoparticles is shown in Fig. 2. After the initial burst release in the first 3 h, the release rate slowed. The profile indicates > 80% of the total formoterol release occurred within the first 24 h with > 99% of the drug release having occurred within the first 48 h.

RPTC Viability

Formoterol has been shown to induce MB in RPTCs at concentrations as low as 10 nM (15). Confluent primary cultures of RPTC (n = 5 biological replicates) exposed to either formoterol free drug or nanoparticles at concentrations up to 100 × the intended 10 nM exposure were assessed for any cytotoxic effects using the resazurin reduction assay. The viability of RPTC exposed to formoterol concentrations (ranged from 3.4×10^{-7} to 3.4×10^{-4} mg/mL, equivalent to 1–1000 nM) (Fig. 3a) did not decrease compared to the control following 24 h of exposure. The viability of proximal tubule cells exposed to nanoparticle concentrations (0.001–1 mg/mL) (Fig. 3b) showed no decrease in viability following 24 h of exposure.

Renal Tubule Nanoparticle Uptake and MB in Mice

The 0.04 mg/kg formoterol containing nanoparticle dose was determined following a preliminary dose ranging study where the amount of formoterol per mass of renal cortex was determined following the administration of three concentrations of formoterol containing nanoparticles (0.3 mg/kg, 0.03 mg/kg, and 0.003 mg/kg). The formoterol content in the renal cortex from these mice was compared to that of an intravenous injection of 0.3 mg/kg of formoterol free drug, a dose that has been shown to induce MB in mice (Table I).

To demonstrate renal uptake of nanoparticles, mice were injected with 0.3 mg/kg free formoterol in solution or 0.04 mg/kg formoterol PLGA-PEG nanoparticles. At 24 h post injection, kidneys were harvested. Renal cross sections were prepared and stained with anti-PEG antibody. Proximal tubule localization was evaluated by co-staining with phytohemagglutinin lectin and DAPI. Results from the formoterol free drug stained sections (Fig. 4a–d) showed limited anti-PEG red fluorescence as expected, demonstrating that the staining was not impacted by formoterol or endogenous PEG-like cellular components. Sections from mice dosed with formoterol containing nanoparticles (Fig. 5a–d, representative, n = 5) showed uptake of nanoparticles in renal proximal tubule segments (dotted arrows), while nanoparticles were not observed in endothelial cells or glomeruli (solid arrows). These results show that the nanoparticles are present in the kidney up to 24 h post-administration.

Analysis of the concentration of formoterol in the renal cortex at 3- and 24-h post-administration (n = 4–5) was normalized to the amount of formoterol that was dosed. At the 3-h time point the amount of formoterol was equivalent (Fig. 5e). Free formoterol injections showed a substantial 95% decrease in formoterol concentration by 24 h. In contrast, at 24 h nanoparticles containing formoterol were decreased by 68% compared to the 3-h time point and were 10 times higher than free formoterol concentrations.

The renal cortex and left ventricle of mice (n = 8–9) injected with free formoterol (0.3 mg/kg) or formoterol containing nanoparticles (0.04 mg/kg formoterol) were assessed following 24 h of exposure for protein biomarkers of MB. In the renal cortex, the master regulator of MB, PGC-1α, was increased 1.3–1.5-fold for free formoterol as well as formoterol containing nanoparticles compared to vehicle control (Fig. 6a). Content of the complex I electron transport chain proteins NADH dehydrogenase 1 (ND1) and NADH:Ubiquinone Oxidoreductase Core Subunit S1 (NDUFS1) increased the renal cortex of mice treated with free formoterol and formoterol containing nanoparticles (Fig. 6 b and c). However, ND1 protein levels in the renal cortex were not increased in formoterol containing nanoparticles.

In the left ventricle, PGC-1α, ND1, and NDUFS1 were not increased in formoterol containing nanoparticles compared to vehicle control (Fig. 6 d, e, f). However, mice treated with free formoterol exhibited an increase in ND1 and NDUFS1 compared to controls (Fig. 6e–f).

To assess MB directly, mice (n = 9–10) were treated with vehicle, free formoterol, or formoterol containing nanoparticles for 24 h. Following treatment, renal cortical tissue was

extracted, stained, and imaged using TEM (Fig. 7a–c). The tissue sections from mice treated with either free formoterol or formoterol containing nanoparticles displayed a 1.4- and 1.8-fold increase, respectively, in the number of mitochondria per field compared to control (Fig. 7d). Additionally, the total mitochondrial area per field was increased 1.4- and 1.5-fold for free formoterol and formoterol containing nanoparticle groups, respectively (Fig. 7e), confirming MB in the treatment groups.

DISCUSSION

Renal targeting of nano-pharmaceuticals is of significant interest for both acute and chronic kidney disease. Nanoparticles have been synthesized to target the glomeruli, relying on nanoparticles being large enough to pass through the endothelial fenestrae but not the glomerular basement membrane, a size range of 10–80 nm (57). Glomerular targeting for formoterol drug delivery is limited in that while formoterol can induce MB in podocytes, the cells of the glomeruli lack the mitochondrial density and energy needs of the proximal tubules (18, 20). Additionally, diseases which impact glomerular filtration will likely alter the efficiency of this mechanism of targeting. Successful nanoparticle targeting of the proximal tubules has been more limited. Previous studies suggested that nanoparticles synthesized between 300 and 500 nm in diameter could localize to the proximal tubules with a high degree of selectivity (46–48). Here we demonstrate that a modified oil-in-water single emulsion can produce PEGylated nanoparticles within the size range, 442 ± 17 nm, required for targeting of the renal tubules. The formoterol encapsulated in PLGA-PEG nanoparticles exhibited *in vitro* sustained release of drug over 24 h, which likely contributed to the prolonged residence time of formoterol within the kidneys. Further, an assessment of the cytotoxicity of both formoterol (1–1000 nM) and the polymeric nanoparticle vehicle (0.001–1 mg/mL) showed a lack of any adverse effects on RPTC viability. Given that formoterol treatment results in the desired MB at 10 nM in RPTCs, this demonstrates that a two order of magnitude increase from targeted dose would not be cytotoxic.

Localization of the nanoparticles to the proximal tubules of the kidneys was assessed in mice treated with vehicle, free formoterol, or encapsulated formoterol PLGA-PEG nanoparticles 24 h following administration. Differences in formoterol content present in the renal cortex between the dosage forms at the 3-h time point were not significant. This is potentially due to the mechanism by which formoterol is eliminated, 54% unchanged by urinary excretion in rats (35), making difficult to differentiate between encapsulated formoterol in the nanoparticles and formoterol being eliminated. However, evaluation of fluorescently conjugated antibody staining of the PEG moiety on the surface of the nanoparticles along with co-staining of tubular endothelial cells with leptin PAH shows uptake of the nanoparticles by the proximal tubules. These sections were taken 24 h post injection and provide evidence that the presence of the nanoparticles in the kidneys is not transient. This is confirmed by the substantial fraction of the formoterol dose remaining in the kidneys of nanoparticle-treated mice at the 24-h time point and indicates that the alteration in the elimination of formoterol from the kidneys is the result of the uptake of PLGA-PEG nanoparticles by the renal tubules.

The mechanism by which these nanoparticles localize to the kidneys has not been fully characterized. The nanoparticles studied here are significantly greater in size than the 80 nm particles which have been shown to localize to the glomeruli (57) suggesting that these particles would not pass through the glomerular basement membrane. This is confirmed by the fluorescent staining of the renal sections which shows significantly less anti-PEG fluorescence in the glomeruli. One potential mechanism previously presented is that particles in this size range are transcytosed by the peritubular endothelial cells into the tubulointerstitial space where they are endocytosed by the tubule epithelial cells (46, 58). This proposed transport is in agreement with the data presented here, which shows a high degree of formoterol retention within the renal cortex and limited evidence of nanoparticles present in the lumen of the tubules or glomeruli. As PLGA-PEG nanoparticles are well known to be biodegradable, it is likely that the route of elimination of these particles will follow hydrolysis of the PLGA backbone.

Mice treated with formoterol PLGA-PEG nanoparticles showed an increase in protein markers of MB as well as new mitochondria that is comparable to intravenous formoterol treatment at significantly higher doses. Our laboratory has previously shown that formoterol treatment is responsible for this MB via overexpression of PGC-1α in renal cortex (10, 15, 17). In this study, we confirm that PGC-1α is induced to a similar degree with encapsulated formoterol PLGA-PEG nanoparticles at a total formoterol dose (0.04 mg/kg), an order of magnitude less than previously reported. The lack of increased renal ND1 expression with formoterol containing nanoparticles is potentially due to pharmacokinetic differences between the free drug and nanoparticle formulations resulting in increased ND1 expression that is not captured by the 24-h time point. Additionally, increased ETC protein expression in the renal cortex suggests that increased PGC-1α resulted in MB which was confirmed by electron microscopy to be similar for both free formoterol, as well as encapsulated formoterol PLGA-PEG nanoparticles even though the nanoparticles contained an 8-fold lower dose of formoterol.

The potential toxicity of repeated formoterol free drug administration is largely related to adverse cardiac effects of β_2 adrenoceptor agonism (25, 59, 60). While a single intravenous dose of formoterol will not result in hypertrophy or other cardiac remodeling within 24 h, stimulation of β_2 adrenoceptor-dependent signaling pathways over time could result in toxicity (22, 23, 61). Increased expression of ETC proteins in the left ventricle of mice treated with formoterol confirms MB. In contrast, the lack of MB from formoterol containing polymeric nanoparticles is likely due to the combined effects of improved localization of formoterol containing nanoparticles to the kidneys and the lower overall dose. Further studies are necessary to confirm the amelioration of any cardiac toxicity with repeated formoterol administration and evaluate the potential of localization of formoterol PLGA-PEG nanoparticles in models of renal injury.

CONCLUSIONS

The β_2-adrenergic receptor is highly expressed in the renal proximal tubules, and activation of this receptor by formoterol has shown significant stimulation of MB as well as improvement in renal function following injury. This study demonstrated that biocompatible

biodegradable polymeric nanoparticles encapsulating formoterol can be successfully and reproducibly synthesized using a modified oil-in-water emulsion solvent evaporation technique. Furthermore, the physicochemical properties and *in vitro* release properties were successfully tailored for this application. These nanoparticles have further been demonstrated to distribute to the renal tubules of mice, thus improving both the localization and retention of formoterol in the target tissue for up to 24 h. Overall, this indicates that the formoterol entrapped nanoparticles have potential as a therapeutic platform for the targeted delivery of biogenic agents in renal injuries mediated by mitochondrial dysfunction such as ischemia-reperfusion–induced kidney injury.

ACKNOWLEDGEMENTS

The authors gratefully acknowledge University of Arizona funding. The authors are grateful to Yelena Feinstein and Krishna Parsawar for assistance with the mass spectrometry as well as the laboratory of Dr. Jianqin Lu for use of their rotary evaporator.

FUNDING

This work was funded in part by support from the University of Arizona College of Pharmacy as well as the Southwest Environmental Health Sciences Center (P30 ES006694).

All SEM images and data were collected in the W.M. Keck Center for Nano-Scale Imaging in the Department of Chemistry and Biochemistry at the University of Arizona with funding from the W.M. Keck Foundation Grant.

All TEM images and data were collected in The University of Arizona, Imaging Cores - Life Sciences North with funding from the NIH (S10 OD011981) and assistance from Dr. William A. Day.

Mass Spectra were acquired by the Arizona Analytical and Biological Mass Spectrometry Core Facility supported by NIEHS grant ES06694 to the Southwest Environmental Health Sciences Center, NIH/NCI grant CA023074 to the Arizona Cancer Center, and by the BIO5 Institute of the University of Arizona.

REFERENCES

1. Feldkamp T, Kribben A, Weinberg JM. Assessment of mitochondrial membrane potential in proximal tubules after hypoxia-reoxygenation. Am J Physiol Ren Physiol. 2005;288(6):F1092–102.
2. Honda HM, Korge P, Weiss JN. Mitochondria and ischemia/reperfusion injury. Ann N Y Acad Sci. 2005;1047:248–58. [PubMed: 16093501]
3. Cleveland KH, Brosius FC, Schnellmann RG. Regulation of mitochondrial dynamics and energetics in the diabetic renal proximal tubule by the β2-adrenergic receptor agonist formoterol. Am J Physiol Ren Physiol. 2020;319(5):F773–F9.
4. Bellomo R, Kellum JA, Ronco C. Acute kidney injury. Lancet. 2012;380(9843):756–66. [PubMed: 22617274]
5. Bhargava P, Schnellmann RG. Mitochondrial energetics in the kidney. Nat Rev Nephrol. 2017;13(10):629–46. [PubMed: 28804120]
6. Rasbach KA, Schnellmann RG. Signaling of mitochondrial biogenesis following oxidant injury. J Biol Chem. 2007;282(4):2355–62. [PubMed: 17116659]
7. Weinberg JM, Venkatachalam MA, Roeser NF, Nissim I. Mitochondrial dysfunction during hypoxia/reoxygenation and its correction by anaerobic metabolism of citric acid cycle intermediates. Proc Natl Acad Sci U S A. 2000;97(6):2826–31. [PubMed: 10717001]
8. Coca SG, Yusuf B, Shlipak MG, Garg AX, Parikh CR. Long-term risk of mortality and other adverse outcomes after acute kidney injury: a systematic review and meta-analysis. Am J Kidney Dis. 2009;53(6):961–73. [PubMed: 19346042]
9. Golestaneh L, Melamed ML, Hostetter TH. Uremic memory: the role of acute kidney injury in long-term outcomes. Kidney Int. 2009;76(8):813–4. [PubMed: 19789540]

10. Rasbach KA, Schnellmann RG. PGC-1alpha over-expression promotes recovery from mitochondrial dysfunction and cell injury. Biochem Biophys Res Commun. 2007;355(3):734–9. [PubMed: 17307137]
11. Bhargava P, Janda J, Schnellmann RG. Elucidation of cGMP-dependent induction of mitochondrial biogenesis through PKG and p38 MAPK in the kidney. Am J Physiol Ren Physiol. 2020;318(2):F322–F8.
12. Dupre TV, Jenkins DP, Muise-Helmericks RC, Schnellmann RG. The 5-hydroxytryptamine receptor 1F stimulates mitochondrial biogenesis and angiogenesis in endothelial cells. Biochem Pharmacol. 2019;169:113644. [PubMed: 31542386]
13. Scarpulla RC. Transcriptional paradigms in mammalian mitochondrial biogenesis and function. Physiol Rev. 2008;88(2):611–38. [PubMed: 18391175]
14. Funk JA, Odejinmi S, Schnellmann RG. SRT1720 induces mitochondrial biogenesis and rescues mitochondrial function after oxidant injury in renal proximal tubule cells. J Pharmacol Exp Ther. 2010;333(2):593–601. [PubMed: 20103585]
15. Wills LP, Trager RE, Beeson GC, Lindsey CC, Peterson YK, Beeson CC, et al. The β2-adrenoceptor agonist formoterol stimulates mitochondrial biogenesis. J Pharmacol Exp Ther. 2012;342(1):106–18. [PubMed: 22490378]
16. Cameron RB, Peterson YK, Beeson CC, Schnellmann RG. Structural and pharmacological basis for the induction of mitochondrial biogenesis by formoterol but not clenbuterol. Sci Rep. 2017;7(1):10578. [PubMed: 28874749]
17. Jesinkey SR, Funk JA, Stallons LJ, Wills LP, Megyesi JK, Beeson CC, et al. Formoterol restores mitochondrial and renal function after ischemia-reperfusion injury. J Am Soc Nephrol. 2014;25(6):1157–62. [PubMed: 24511124]
18. Cameron RB, Gibbs WS, Miller SR, Dupre TV, Megyesi J, Beeson CC, et al. Proximal Tubule. J Pharmacol Exp Ther. 2019;369(1):173–80. [PubMed: 30709866]
19. Arif E, Solanki AK, Srivastava P, Rahman B, Fitzgibbon WR, Deng P, et al. Mitochondrial biogenesis induced by the β2-adrenergic receptor agonist formoterol accelerates podocyte recovery from glomerular injury. Kidney Int. 2019;96(3):656–73. [PubMed: 31262488]
20. Boivin V, Jahns R, Gambaryan S, Ness W, Boege F, Lohse MJ. Immunofluorescent imaging of beta 1- and beta 2-adrenergic receptors in rat kidney. Kidney Int. 2001;59(2):515–31. [PubMed: 11168934]
21. Arif E, Nihalani D. Beta2-adrenergic receptor in kidney biology: A current prospective. Nephrology (Carlton). 2019;24(5):497–503. [PubMed: 30848004]
22. Levine MA, Leenen FH. Role of beta 1-receptors and vagal tone in cardiac inotropic and chronotropic responses to a beta 2-agonist in humans. Circulation. 1989;79(1):107–15. [PubMed: 2562936]
23. Brodde OE. Beta 1- and beta 2-adrenoceptors in the human heart: properties, function, and alterations in chronic heart failure. Pharmacol Rev. 1991;43(2):203–42. [PubMed: 1677200]
24. Vyas FS, Nelson CP, Freeman F, Boocock DJ, Hargreaves AJ, Dickenson JM. β 2-adrenoceptor-induced modulation of transglutaminase 2 transamidase activity in cardiomyoblasts. Eur J Pharmacol. 2017;813:105–21. [PubMed: 28754379]
25. Molenaar P, Chen L, Parsonage WA. Cardiac implications for the use of beta2-adrenoceptor agonists for the management of muscle wasting. Br J Pharmacol. 2006;147(6):583–6. [PubMed: 16432500]
26. Yin Q, Yang C, Wu J, Lu H, Zheng X, Zhang Y, et al. Downregulation of β-adrenoceptors in isoproterenol-induced cardiac remodeling through HuR. PLoS One. 2016;11(4):e0152005. [PubMed: 27035432]
27. Koziczak-Holbro M, Rigel DF, Dumotier B, Sykes DA, Tsao J, Nguyen NH, et al. Pharmacological characterization of a novel 5-hydroxybenzothiazolone-derived. J Pharmacol Exp Ther. 2019;369(2):188–99. [PubMed: 30819762]
28. Mansour HM, Sohn M, Al-Ghananeem A, P PD Materials for pharmaceutical dosage forms: molecular pharmaceutics and controlled release drug delivery aspects. . International Journal of Molecular Sciences. 2010;11(special issue-material sciences and nanotechnology section - biodegradability of materials.):3298–32 [PubMed: 20957095]

29. Makadia HK, Siegel SJ. Poly Lactic-co-Glycolic Acid (PLGA) as biodegradable controlled drug delivery carrier. Polymers (Basel). 2011;3(3):1377–97. [PubMed: 22577513]
30. Rhee YS, Park CW, DeLuca PP, Mansour HM. Sustained-release injectable drug delivery systems. . Pharmaceutical Technology: Special Issue-Drug Delivery. 2010(11): 6–13
31. Hasanpour A, Esmaeili F, Hosseini H, Amani A. Use of mPEG-PLGA nanoparticles to improve bioactivity and hemocompatibility of streptokinase: in-vitro and in-vivo studies. Mater Sci Eng C Mater Biol Appl. 2021;118:111427. [PubMed: 33255024]
32. Muralidharan P, Mallory E, Malapit M, Hayes D Jr, Mansour HM. Inhalable PEGylated phospholipid nanocarriers and PEGylated therapeutics for respiratory delivery as aerosolized colloidal dispersions and dry powder inhalers. Pharmaceutics. 2014;6(2):333–53. [PubMed: 24955820]
33. Duncan R, Gaspar R. Nanomedicine(s) under the microscope. Mol Pharm. 2011;8(6):2101–41. [PubMed: 21974749]
34. Singh R, Lillard JW. Nanoparticle-based targeted drug delivery. Exp Mol Pathol. 2009;86(3):215–23. [PubMed: 19186176]
35. Sasaki H, Kamimura H, Shiobara Y, Esumi Y, Takaichi M, Yokoshima T. Disposition and metabolism of formoterol fumarate, a new bronchodilator, in rats and dogs. Xenobiotica. 1982;12(12):803–12. [PubMed: 7170790]
36. Labhasetwar V, Song C, Humphrey W, Shebuski R, Levy RJ. Arterial uptake of biodegradable nanoparticles: effect of surface modifications. J Pharm Sci. 1998;87(10):1229–34. [PubMed: 9758682]
37. Kumar A, Mansour HM, Friedman A, Blough E. Nanomedicine in Drug Delivery. 1st ed: CRC Press; 2017
38. Wang AZ, Langer R, Farokhzad OC. Nanoparticle delivery of cancer drugs. Annu Rev Med. 2012;63:185–98. [PubMed: 21888516]
39. Song CX, Labhasetwar V, Murphy H, Qu X, Humphry WR, Shebuski RJ, et al. Formulation and characterization of biodegradable nanoparticles for intravascular local drug delivery. J Control Release. 1997;43:197–212.
40. Westedt U, Kalinowski M, Wittmar M, Merdan T, Unger F, Fuchs J, et al. Poly(vinyl alcohol)-graft-poly(lactide-co-glycolide) nanoparticles for local delivery of paclitaxel for restenosis treatment. J Control Release. 2007;119(1):41–51. [PubMed: 17346845]
41. He J, Chen H, Zhou W, Chen M, Yao Y, Zhang Z, et al. Kidney targeted delivery of asiatic acid using a FITC labeled renal tubular-targeting peptide modified PLGA-PEG system. Int J Pharm. 2020;584:119455. [PubMed: 32464235]
42. Yu H, Lin T, Chen W, Cao W, Zhang C, Wang T, et al. Size and temporal-dependent efficacy of oltipraz-loaded PLGA nanoparticles for treatment of acute kidney injury and fibrosis. Biomaterials. 2019;219:119368. [PubMed: 31349200]
43. Mansour HM, Park CW. Book Chapter: Therapeutic and clinical aspects of nanomedicines and nanopharmaceutical products. In: Brenner S, editor. The Nanomedicine Handbook for Clinicians 1. London. United Kingdom: CRC Press, Inc.; 2011.
44. Williams RM, Jaimes EA, Heller DA. Nanomedicines for kidney diseases. Kidney Int. 2016;90(4):740–5. [PubMed: 27292222]
45. Nair AV, Keliher EJ, Core AB, Brown D, Weissleder R. Characterizing the interactions of organic nanoparticles with renal epithelial cells in vivo. ACS Nano. 2015;9(4):3641–53. [PubMed: 25790730]
46. Williams RM, Shah J, Ng BD, Minton DR, Gudas LJ, Park CY, et al. Mesoscale nanoparticles selectively target the renal proximal tubule epithelium. Nano Lett. 2015;15(4):2358–64. [PubMed: 25811353]
47. Williams RM, Shah J, Tian HS, Chen X, Geissmann F, Jaimes EA, et al. Selective Nanoparticle Targeting of the Renal Tubules. Hypertension. 2018;71(1):87–94. [PubMed: 29133360]
48. Han SJ, Williams RM, D'Agati V, Jaimes EA, Heller DA, Lee HT. Selective nanoparticle-mediated targeting of renal tubular Toll-like receptor 9 attenuates ischemic acute kidney injury. Kidney Int. 2020;98(1):76–87. [PubMed: 32386967]

49. Zhang Z, Feng SS. The drug encapsulation efficiency, in vitro drug release, cellular uptake and cytotoxicity of paclitaxel-loaded poly(lactide)-tocopheryl polyethylene glycol succinate nanoparticles. Biomaterials. 2006;27(21):4025–33. [PubMed: 16564085]
50. Duan JH, Mansour HM, Zhang YD, Deng XM, Zhao JF. Reversion of multi-drug resistance by co-encapsulation of doxorubicin and curcumin in chitosan/poly(butylcyanoacrylate) nanoparticles. Int J Pharm. 2012:1–9.
51. Mascher DG, Zech K, Nave R, Kubesch KM, Mascher HJ. Ultra-sensitive determination of Formoterol in human serum by high performance liquid chromatography and electrospray tandem mass spectrometry. J Chromatogr B Anal Technol Biomed Life Sci. 2006;830(1):25–34.
52. Alabsi W, Al-Obeidi FA, Polt R, Mansour HM. Organic solution advanced spray-dried microparticulate/nanoparticulate dry powders of lactomorphin for respiratory delivery: physicochemical characterization, in vitro aerosol dispersion, and cellular studies. Pharmaceutics. 2021;13:26.
53. Park CW, Li X, Vogt FG, Hayes D Jr, Zwischenberger JB, Park ES, et al. Advanced spray-dried design, physicochemical characterization, and aerosol dispersion performance of vancomycin and clarithromycin multifunctional controlled release particles for targeted respiratory delivery as dry powder inhalation aerosols. Int J Pharm. 2013;455(1–2):374–92. [PubMed: 23820131]
54. Nowak G, Schnellmann RG. Improved culture conditions stimulate gluconeogenesis in primary cultures of renal proximal tubule cells. Am J Phys. 1995;268(4 Pt 1):C1053–61.
55. Acosta MF, Abrahamson MD, Encinas-Basurto D, Fineman JR, Black SM, Mansour HM. Inhalable nanoparticles/microparticles of an AMPK and Nrf2 activator for targeted pulmonary drug delivery as dry powder inhalers. AAPS J. 2020;23(1):2. [PubMed: 33200330]
56. Isoe J, Collins J, Badgandi H, Day WA, Miesfeld RL. Defects in coatomer protein I (COPI) transport cause blood feeding-induced mortality in yellow fever mosquitoes. Proc Natl Acad Sci U S A. 2011;108(24):E211–7. [PubMed: 21628559]
57. Zuckerman JE, Davis ME. Targeting therapeutics to the glomerulus with nanoparticles. Adv Chronic Kidney Dis. 2013;20(6):500–7. [PubMed: 24206602]
58. Cartiera MS, Johnson KM, Rajendran V, Caplan MJ, Saltzman WM. The uptake and intracellular fate of PLGA nanoparticles in epithelial cells. Biomaterials. 2009;30(14):2790–8. [PubMed: 19232712]
59. Bernstein D, Fajardo G, Zhao M. The role of β-adrenergic receptors in heart failure: differential regulation of cardiotoxicity and cardioprotection. Prog Pediatr Cardiol. 2011;31(1):35–8. [PubMed: 21765627]
60. Brouri F, Findji L, Mediani O, Mougenot N, Hanoun N, Le Naour G, et al. Toxic cardiac effects of catecholamines: role of beta-adrenoceptor downregulation. Eur J Pharmacol. 2002;456(1–3):69–75. [PubMed: 12450571]
61. de Zeeuw D, Akizawa T, Audhya P, Bakris GL, Chin M, Christ-Schmidt H, et al. Bardoxolone methyl in type 2 diabetes and stage 4 chronic kidney disease. N Engl J Med. 2013;369(26):2492–503. [PubMed: 24206459]

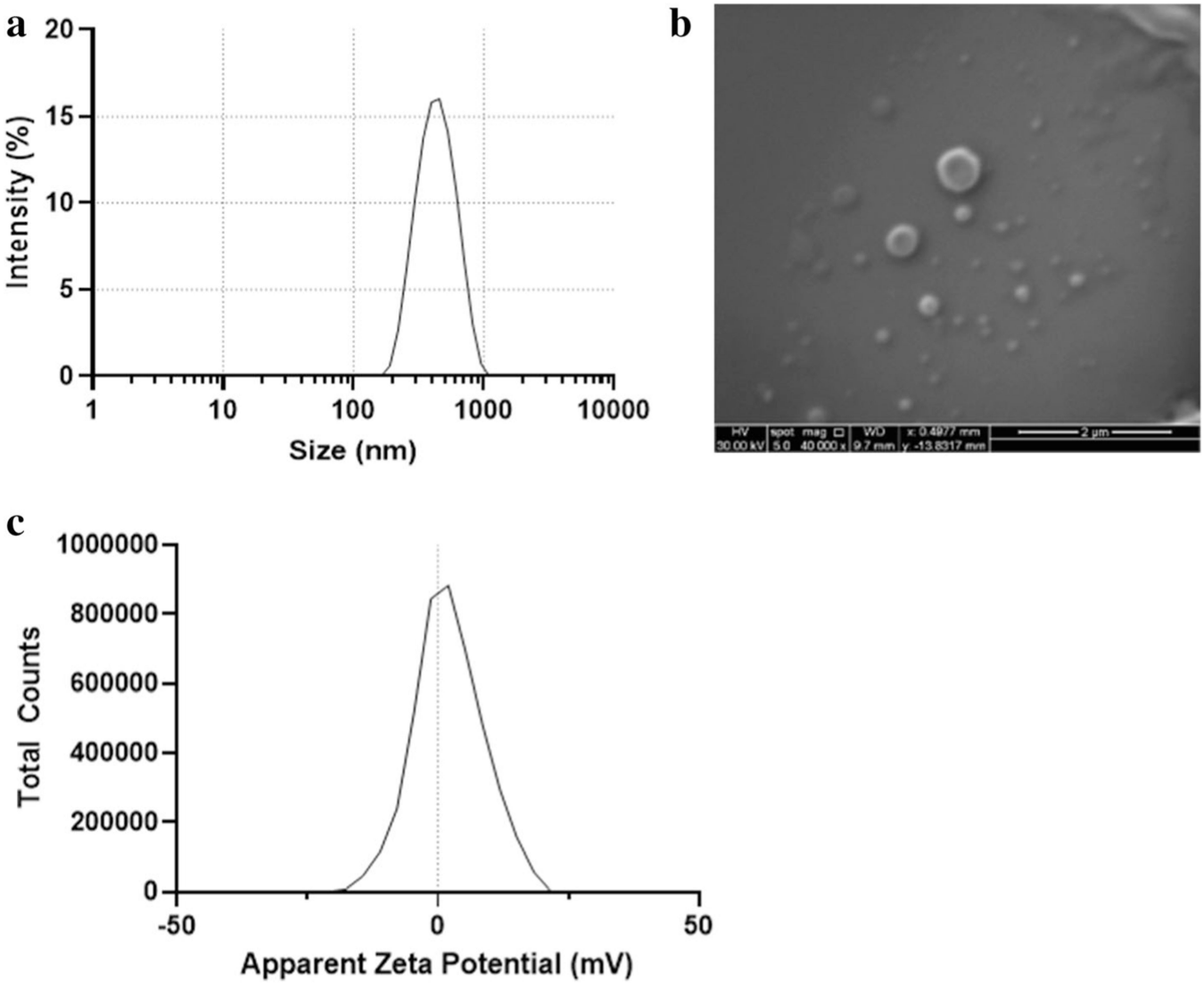

Fig. 1.

Nanoparticles (NP) containing formoterol were prepared as described. **a** NP hydrodynamic diameter was measured via dynamic light scattering (DLS) using the Malvern Zetasizer Nano ZS. Size distribution is representative (n = 3). **b** NP size and morphology was assessed via SEM. **c** Zeta potential was determined at a concentration of 0.1 mg/mL of NP suspended in 0.1× normal saline at 25°C and a measured pH of 7.2. Zeta potential is representative (n = 3)

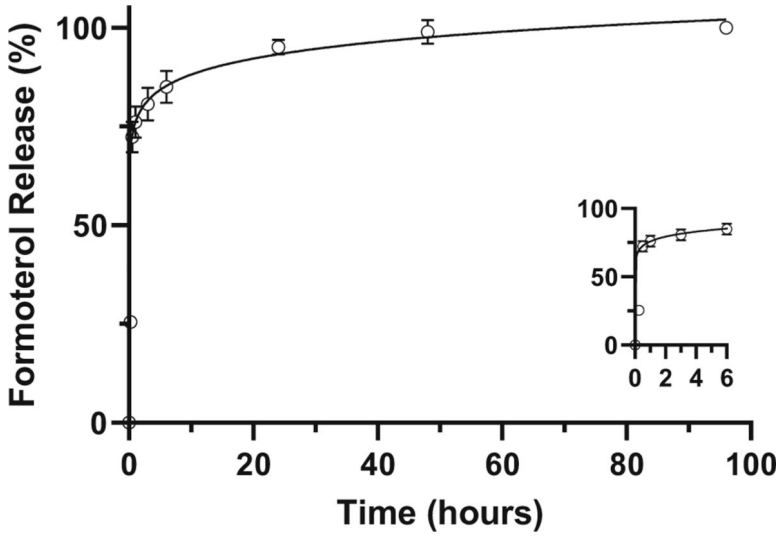

Fig. 2.

Cumulative formoterol release from nanoparticle suspension over time. Nanoparticles containing formoterol are dispersed in 1× PBS with stirring at 37°C. Data is presented as mean ± s.d. (n = 3)

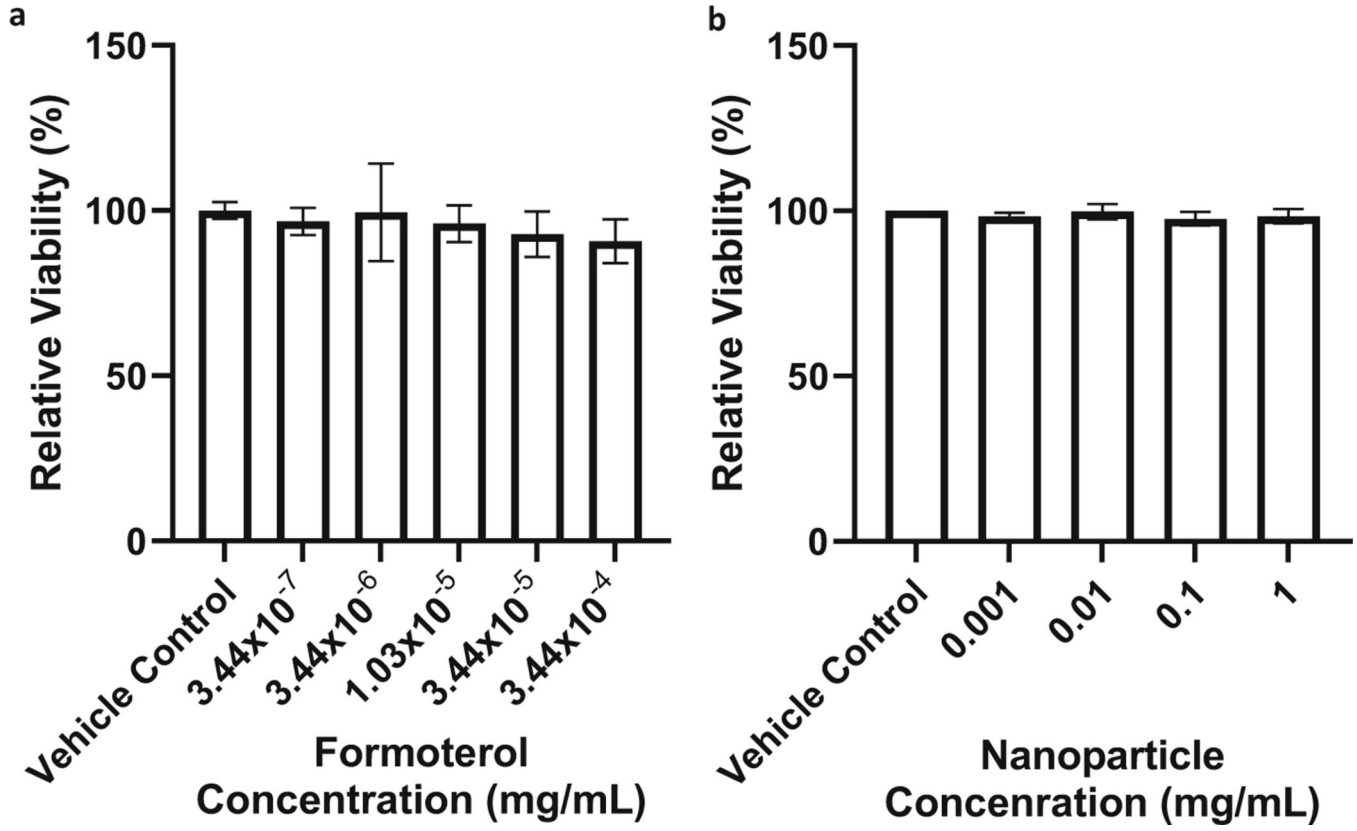

Fig. 3.

a Formoterol and **b** PLGA-PEG nanoparticles (NP) do not impact viability of renal proximal tubule cells (RPTCs). After reaching confluence, cells were exposed to either formoterol or PLGA-PEG NP at concentrations from 1 to 1000 nM (formoterol) or 0.001 to 1 mg/mL (NP) for 24 h. After 24 h of exposure, cells were washed with fresh media and viability was assessed by resazurin assay. Data were analyzed via one-way ANOVA followed by Dunnett's post hoc test to evaluate differences between groups. Data are presented as the mean of ± s.d. (n = 5 biological replicates). ns, no significant difference versus vehicle control

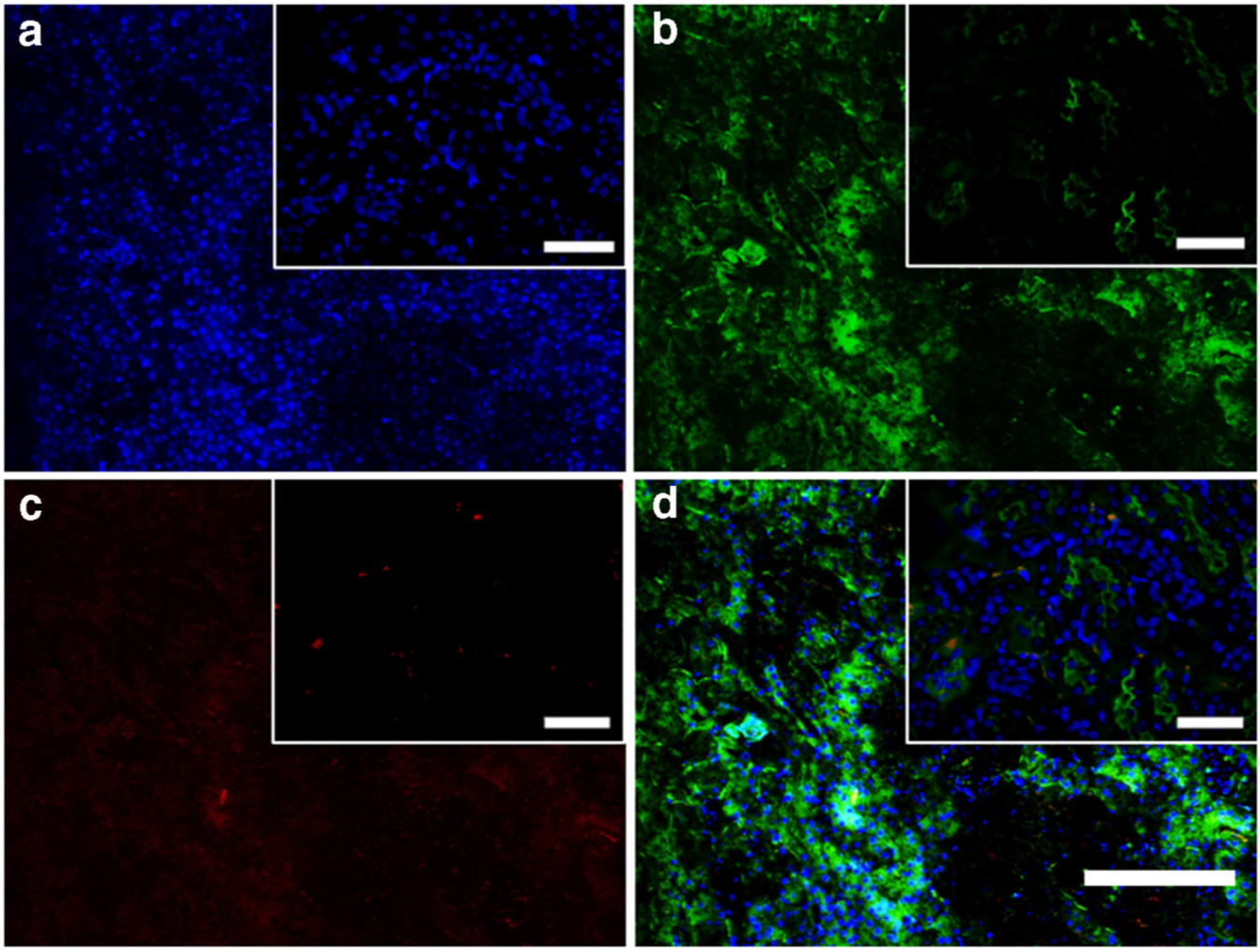

Fig. 4.

Renal cross sections of formoterol free drug treated mice are co-stained with **a** 40,6-diamidino-2-phenylindole (DAPI) to visualize cell nuclei (blue), **b** phytohemagglutinin (PHA) lectin to identify renal proximal tubules (green), and **c** anti-polyethylene glycol (PEG) antibody to visualize nanoparticles. **d** Merged image. Scale bar on full scale image is 150 μm, scale bar in magnified inserts is 50 μm

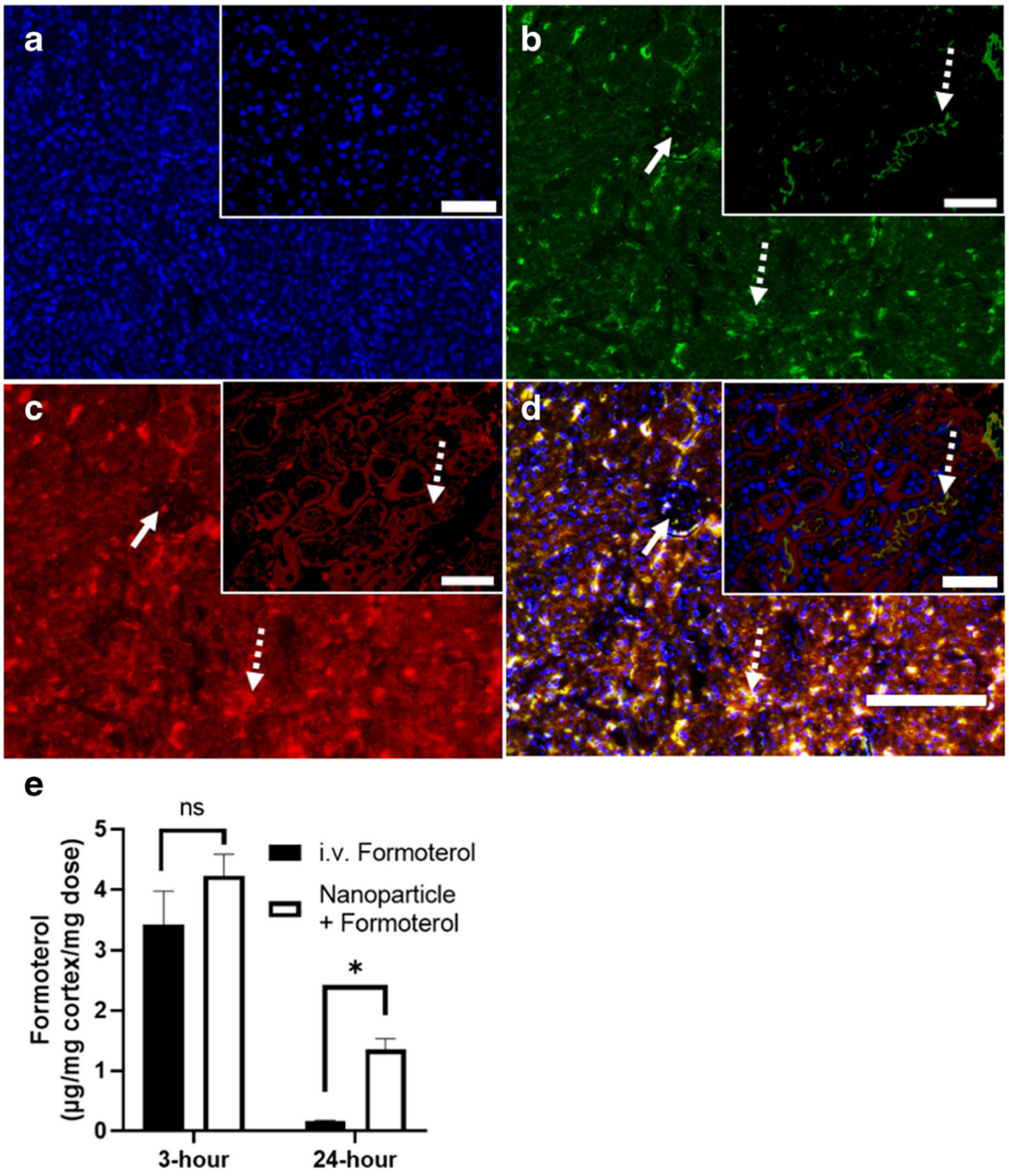

Fig. 5.

Evaluation of NP renal localization. Renal cross sections are co-stained with **a** 40,6-diamidino-2-phenylindole (DAPI) to visualize cell nuclei (blue), **b** phytohemagglutinin (PHA) lectin to identify renal proximal tubules (green), and **c** anti-polyethylene glycol (PEG) antibody to visualize nanoparticles. **d** Merged image. Solid arrows identify glomeruli, dotted arrows identify proximal tubules. Scale bar on full scale image is 150 µm, scale bar in magnified inserts is 50 µm. **e** Formoterol concentration in renal cortex as determined by LCMS-MS at 3- and 24-h post-administration. Data were analyzed via Student's t-tests to

evaluate differences between groups. Data are presented as the mean ± s.d. (n = 4–5). → $P<0.05$, ns indicates no significance between groups

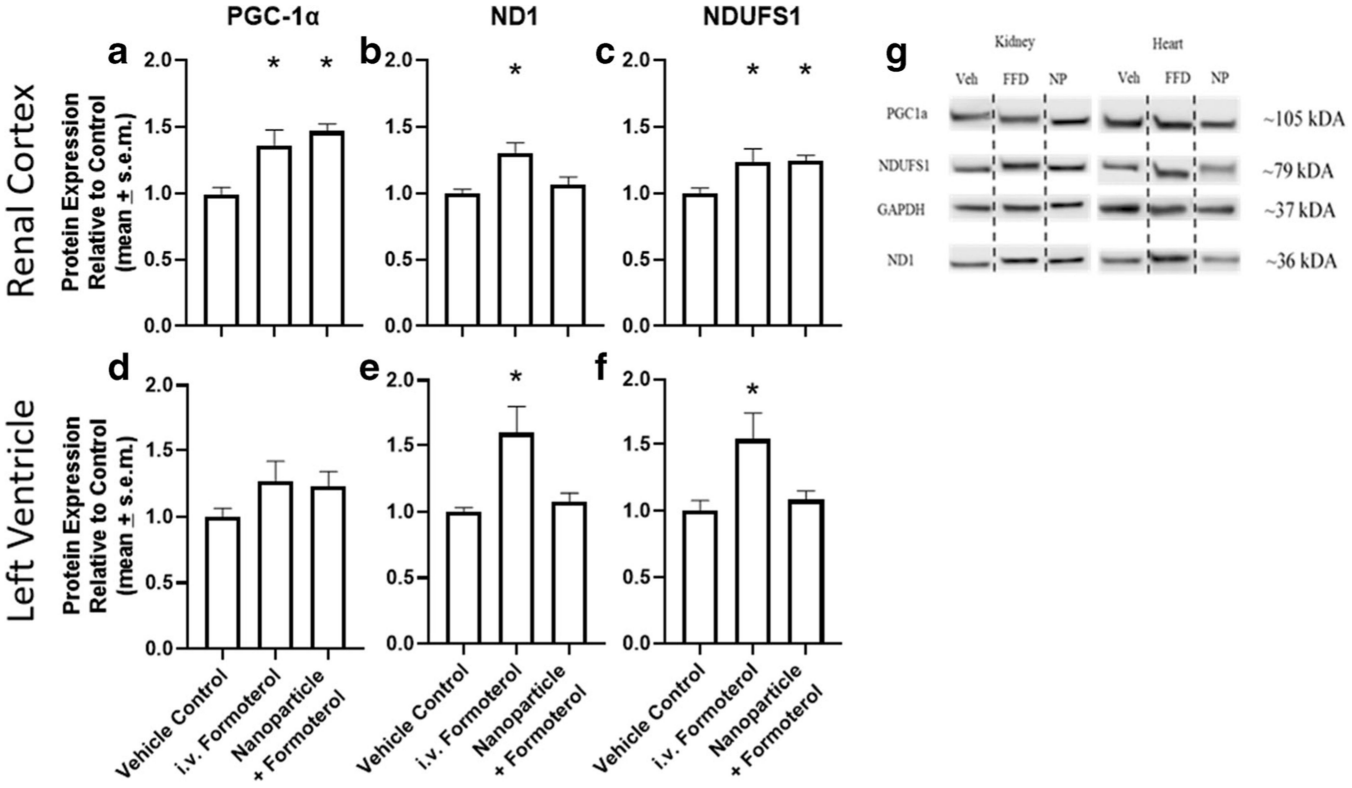

Fig. 6.

Nanoparticles containing formoterol stimulate mitochondrial biogenesis. C57Bl/6 mice received a single lateral tail vein injection of either vehicle, formoterol (0.3 mg/kg), or formoterol containing nanoparticle (0.04 mg/kg formoterol). Renal cortex (**a–c**) and left ventricle (**d–f**) was evaluated by immunoblotting for PGC1a (**a** and **d**), ND1 (**b** and **e**) and NDUFS1 (**c** and **f**) expression and quantified via densitometry. **g** Representative immunoblots. Data were analyzed via one-way ANOVA followed by Dunnett's post hoc test to evaluate differences between groups. Data are presented as the mean of + s.e.m. (n = 8–9). *P, 0.05 versus vehicle control, FFD is free formoterol, NP is formoterol encapsulated nanoparticles

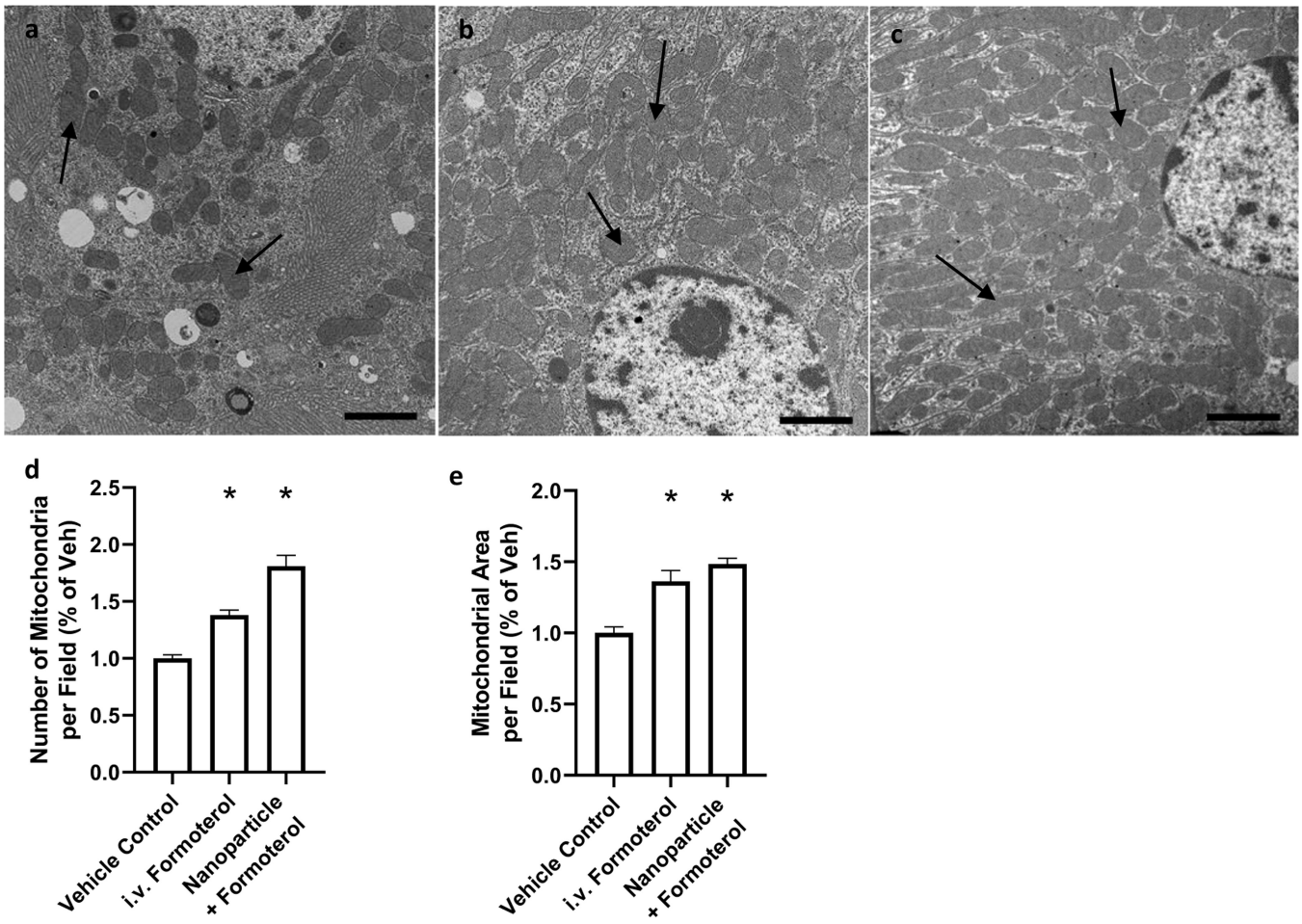

Fig. 7.

Representative electron micrographs of renal cortical sections from mice exposed to either **a** vehicle control, **b** 0.3 mg/kg formoterol, **c** 0.04 mg/kg formoterol NP. **d** Quantification of mitochondria (black arrows) per field. **e** Quantification of total mitochondrial area per field. Data were analyzed via one-way ANOVA followed by Dunnett's post hoc test to evaluate differences between groups. Arrows indicate mitochondria. Data are presented as the mean of + s.e.m. (n = 5). *P, 0.05 versus vehicle control

Table I.

Renal Formoterol Drug Content Following Nanoparticle and Free Drug Dosing. Average Formoterol Recovered Per Mass of Renal Cortex (pg/mg). Mean ± s.d (n = 5)

Dosing formoterol (mg/kg)		Average formoterol (pg/mg)
Formoterol nanoparticle	0.3	81.5 ± 10.5
Formoterol nanoparticle	0.03	27.6 ± 3.1
Formoterol nanoparticle	0.003	1.5 ± 1.0
Formoterol free drug	0.3	33.2 ± 5.0